

The Importance of Lattice Defects in Katanin-Mediated Microtubule Severing in Vitro

Liza J. Davis,* David J. Odde,[†] Steven M. Block,[‡] and Steven P. Gross[§]

Departments of *Chemical Engineering and Materials Science and [†]Biomedical Engineering, University of Minnesota, Minneapolis, Minnesota 55455; [‡]Department of Biological Sciences, Stanford University, Stanford, California 94305; and [§]Department of Developmental and Cell Biology, University of California-Irvine, Irvine, California 92697 USA

ABSTRACT The microtubule-severing enzyme katanin uses ATP hydrolysis to disrupt noncovalent bonds between tubulin dimers within the microtubule lattice. Although its microtubule severing activity is likely important for fundamental processes including mitosis and axonal outgrowth, its mechanism of action is poorly understood. To better understand this activity, an in vitro assay was developed to enable the real-time observation of katanin-mediated severing of individual, mechanically unconstrained microtubules. To interpret the experimental observations, a number of theoretical models were developed and compared quantitatively to the experimental data via Monte Carlo simulation. Models that assumed that katanin acts on a uniform microtubule lattice were incompatible with the in vitro data, whereas a model that assumed that katanin acts preferentially on spatially infrequent microtubule lattice defects was found to correctly predict the experimentally observed breaking rates, number and spatial frequency of severing events, final levels of severing, and sensitivity to katanin concentration over the range 6–300 nM. As a result of our analysis, we propose that defects in the microtubule lattice, which are known to exist but previously not known to have any biological function, serve as sites for katanin activity.

INTRODUCTION

Katanin, a heterodimer of 60- and 80-kDa subunits (p60 and p80), uses energy from ATP hydrolysis to disrupt tubulin-tubulin contacts within the microtubule (MT) lattice, severing the MT but leaving tubulin capable of subsequent re-polymerization (McNally and Vale, 1993). The observation that katanin is activated during mitosis implies a likely role in the massive disassembly of microtubules before spindle formation (Vale, 1991), and the high level of localization at the centrosome observed throughout the cell cycle is consistent with katanin-mediated depolymerization at the minus-end during metaphase poleward flux (McNally et al., 1996). Microtubule severing by katanin has been shown to play a role in release of MTs from the centrosome of neurons, axonal outgrowth (Ahmad et al., 1999), and severing of doublet MTs in the flagella of *Chlamydomonas* during deflagellation (Lohret et al., 1998).

Katanin is a member of the highly diverse AAA (ATPases associated with different cellular activities) protein superfamily (Hartman et al., 1998), which often act as oligomers and in some cases form hexameric rings (Vale, 2000). In the case of katanin, rotary-shadowing electron microscopy of p60 and of p60/p80 katanin (Hartman et al., 1998) and fluorescence resonance energy transfer (FRET) analysis of p60 have shown that katanin forms a transient hexamer in the presence of both ATP and microtubules (Hartman and Vale, 1999). However, the MT binding site for this hexamer

is unknown. Possible binding sites include the outside of the microtubule, the MT lumen, or the sides of dimers exposed by holes in the lattice (McNally, 2000). The latter two possibilities suggest that katanin might act specifically at points in the lattice that contain defects. A fundamental question is whether katanin acts on all tubulin dimers with equal affinity or acts on specific defective sites within the microtubule lattice.

This question is potentially addressable through light microscopy because it was light microscopy that was used to discover katanin (Vale, 1991). Katanin-mediated microtubule severing has been observed in vitro using fluorescence microscopy to visualize rhodamine-labeled, paclitaxel- or GMPCPP-stabilized MTs attached to a coverslip by *Xenopus* cell extract (Vale, 1991; McNally and Vale, 1993) or a single-headed kinesin mutant (Hartman et al., 1998; McNally, 2000). Within minutes of katanin addition, MTs become visibly fragmented. Similar assays using VE-DIC microscopy have allowed observation of MT kinks, which formed ~90 s after katanin perfusion and became breaks several seconds later (Vale, 1991). Unfortunately, these assays mechanically constrain the microtubules, presumably at random points along their length, and preclude the collection of information about mechanical stresses released from or added to the MTs during severing. In these assays, severing events are noted by observing gaps of 200 nm or greater (~25 rows of tubulin) in the fluorescence. As a result, multiple severing events or severing followed by depolymerization may be necessary to create a gap large enough for detection by fluorescence microscopy.

These issues were eliminated in the present investigation. Here, in vitro microtubule severing by katanin was observed in real time by VE-DIC during assays in which the MTs were constrained only at the nucleating end, allowing the

Submitted September 21, 2001, and accepted for publication December 5, 2001.

Address reprint requests to Dr. David J. Odde, 7-104 BSBE, 312 Church St. SE, Minneapolis, MN 55455. Tel.: 612-626-9980; Fax: 612-626-6583; E-mail: oddex002@umn.edu.

© 2002 by the Biophysical Society

0006-3495/02/06/2916/12 \$2.00

observation of kinks in MTs unconstrained by motor proteins. This new assay for katanin activity also allows a precise determination of when severing is complete: when the MT is fully severed, the distal end promptly diffuses away. Using this assay, severing at two katanin concentrations (290 nM and 5.7 nM) was analyzed to determine the time-scales of kinking and severing, the distribution of kinking angles, and the relationship between the kinked and broken states.

To test whether katanin acts on all dimers with equal affinity or is targeted to specific sites on the microtubules lattice, severing was simulated using several different stochastic severing models. Models in which all katanin-tubulin interactions were equivalent (defect-free lattice models), as well as a model in which katanin activity was localized to random points on the microtubule (defect-containing lattice model) were considered. In addition, the defect-free model was modified so that multiple tubulin dimers were removed with each cycle of katanin activity, the katanin concentration decreased with time, or tubulin was removed cooperatively. Each model was simulated using the same initial MT lengths as were observed in vitro, and these results were directly compared to the experimental data. An acceptable model would predict the appropriate temporal and spatial frequency of severing using a single parameter set for both katanin concentrations. It was determined that defect-free lattice models were inconsistent with observed severing characteristics, while a defect-containing lattice model was consistent with observed severing.

MATERIALS AND METHODS

Tubulin, axoneme, and katanin preparation

Tubulin was purchased from Cytoskeleton, Inc. (Denver, CO) and stored at -70°C . Before each experiment, a small aliquot was thawed, diluted to $20\ \mu\text{M}$ with PEM buffer (80 mM Pipes, 1 mM EGTA, 4 mM MgCl_2 , 1 mM GTP, pH 6.9 by KOH), stored on ice, and used within 1–2 h. Axoneme fragments from *Strongylocentrotus purpuratus* were purified using the method of Bell et al. (1982). Fragments were stored in 50% glycerol at -20°C , washed in PEM buffer, and sonicated in a 400 W cup sonicator at 80% power for five pulses before use. Recombinant p60/p80 sea urchin katanin (gift from James Hartman and Ron Vale) prepared from baculovirus-infected Sf9 cells (Hartman et al., 1998) was diluted from a stock solution (440 mg p60/ml) to 25:1 (290 nM) and 1280:1 (5.7 nM) with HEPES buffer (10 mM HEPES, 1 mM MgCl_2 , 20 μM paclitaxel, 1 mM ATP, pH 7.5) before use.

Microtubule severing assay

A 10- μl perfusion chamber was prepared by adhering a coverslip to a microscope slide with two pieces of double-sided tape placed $\sim 3\ \text{mm}$ apart. Axoneme fragments (10 μl) were perfused and incubated for 10 min to allow them to adhere. Next, a solution of 5 mg/ml casein was perfused and incubated for 3 min. Unattached axonemes were washed out by perfusing $\sim 50\ \mu\text{l}$ PEM buffer through the chamber, followed by perfusion with 10 μl of 20 μM tubulin. After 10 min, microtubules had formed from axoneme ends via self-assembly. Paclitaxel-PEM buffer (10 μl of 20 μM paclitaxel in PEM buffer) was then perfused into the chamber and allowed

to stabilize the MTs. Unpolymerized tubulin was washed out with $\sim 50\ \mu\text{l}$ of paclitaxel-PEM. The perfusion chamber was placed on the microscope and 10 μl katanin was perfused while recording. Fourteen experiments were performed at each concentration of katanin. Due to a lack of observed severing events in several experiments, six assays with 5.7 nM katanin and nine assays with 290 nM katanin were analyzed.

Videomicroscopy

Video-enhanced differential interference contrast (VE-DIC) microscopy was used to observe microtubules during severing. A Zeiss Axiovert 100 inverted microscope with a 100 \times , 1.3 NA planapochromat oil-immersion objective lens and a 1.4 NA oil immersion condenser was used to observe the severing process. Illumination was provided by a 100 W Hg arc lamp, and images were detected and processed by a Hamamatsu C2400 CCD camera and Argus 20 image processor. An S-VHS videotape deck was used to record and time-stamp the images in real time (30 frames/s). Experiments with 5.7 nM katanin were recorded for at least 20 min from the time of katanin perfusion; those with 290 nM katanin were recorded for at least 10 min. Data analysis was performed using an LG-3 frame grabber (Scion Corp., Frederick, MD) to capture frames for analysis and Scion Image (Scion Corp.) to measure microtubule lengths and angles.

Kink and break times

For each severing event, the initial and final lengths of the microtubule were measured using Scion Image. The time of katanin perfusion, the first observable kink, and the final break were noted. Microtubules that could not be observed continuously from perfusion to break were not included in the analysis presented here. The total normalized length (total length/total initial length) was plotted as a function of time for each katanin concentration and called the “microtubule survival curve.”

At each concentration, the distribution of times that microtubules spent in the kinked state was plotted as a cumulative distribution function (CDF) and fit with an exponential by minimizing the sum-of-squares error (SSE) to find the first-order rate constant for the kink-to-break transition, k_{kb} . The probability of fit for the exponential model, p_{exp} , was determined by comparing SSE_{data} to the SSE values calculated from 100 simulated exponential data sets of the same size as the experimental data sets and their best-fit curves: $SSE_{\text{sim}1}, \dots, SSE_{\text{sim}100}$, which were also plotted as a CDF. One minus the percentile at which SSE_{data} fit into the CDF of SSE_{sim} values was the probability of fit.

Angle measurements

After kinking began, the two-dimensional (in focal plane) kinking angle was measured at 0.5-s intervals using Scion Image. Microtubules whose kinked end went out of focus were assumed to be kinking out of the plane, and were not included [$n = 3$]. Kinks that remained in focus $< 80\%$ of the time between the initial formation of the kink and the break [$n = 10$], as well as those that were very short [$n = 3$] or that broke at the axoneme-microtubule junction [$n = 4$] (increasing the uncertainty in angle measurements) were also not included. Depending on the image quality and kinking angle, the standard deviation for any specific angle measurement was between 1° and 5° , typically $\sim 2^{\circ}$ uncertainty.

Diffusion-reaction model for the kink-to-break dynamics

A diffusion-reaction model was fit to the experimentally observed cumulative distribution of kinking angles. In this model, the distal end of a kinked microtubule rotates about a hinge-point, with rotational diffusivity

D_r , before being severed by a first-order reaction with rate constant, k_{kb} . The model can be described by the following diffusion equation:

$$\frac{\partial f}{\partial t} = D_r \frac{\partial^2 f}{\partial \theta^2} - k_{kb} f \quad (1)$$

where f is the probability of the MT segment being oriented at angle θ ($\theta = 0^\circ$ corresponds to a straight MT) at time t . The boundary conditions are 1) $\partial f / \partial \theta = 0$ when $\theta = 0$, and 2) $f = 0$ as $\theta \rightarrow \infty$, with initial condition: $f = \delta(\theta)$. The analytical solution is (Crank, 1975):

$$f(\theta, t) = (\pi D_r t)^{-1/2} \exp[-\theta^2 / 4 D_r t - k_{kb} t] \quad (2)$$

The cumulative distribution function, $F(\theta)$, was calculated from the model by numerically integrating Eq. 2 over all times and all angles from zero to the current angle, θ :

$$F(\theta, t) = \int_0^\theta \int_0^\infty f(\theta, t) dt d\theta \quad (3)$$

The best-fit value for D_r was chosen by minimizing the SSE between a CDF of the observed kinking angles and $F(\theta)$. Because kinks $< 5^\circ$ were not readily discerned by eye, their relative frequency was likely underestimated and they were not included in this analysis. The probability of fit for the diffusion-reaction model, $p_{d,r}$, was determined by simulating 100 additional data sets (created by simulating the rotational diffusion of kinked microtubules about a hinge point using D_r from the experimental fit), finding each best-fit D_r and corresponding SSE, and comparing SSE_{data} to the distribution of SSEs from simulations. All angles were assumed to be energetically equivalent.

Microtubule-severing models

Monte Carlo simulations were implemented using Matlab v. 6.0, release 12. The stochastic severing models simulated the state of 13-protofilament, B-type lattices (represented by $n [l_n \times 13]$ matrices), where n was the number of microtubules simulated and l_n was the number of rows per MT. Simulations used the initial lengths of either the 22 MTs in the 290 nM katanin population or the 10 MTs in the 5.7 nM katanin population to model the predicted behavior of the system.

The matrix representing each microtubule was coded for the state of the dimer locations that it represented: “1” for an intact tubulin, “2” for tubulin with katanin bound, and “0” for a missing tubulin dimer. Each matrix entry was updated at each time step, τ , (τ chosen such that $p_{event} \leq 0.05$) depending on the value of a random number chosen between zero and one. The random number, r , was compared to the probability of a specific event: katanin binding (p_{on}, k_{on}), katanin dissociating (p_{off}, k_{off}), or katanin removing a tubulin dimer as it dissociates (p_{rem}, k_{rem}); if $r < p_{event}$, then the event was assumed to have taken place. The probability of occurrence for each event was calculated from:

$$P_{event} = 1 - \exp[-k_{event} \tau] \quad (4)$$

where k_{event} is the first-order (or pseudo-first-order) rate constant for the event. Simulations began with an intact lattice with no katanin bound, represented by a matrix filled with “1.” As the simulation progressed, the matrix entries were updated to represent the binding and dissociation of katanin and removal of tubulin.

At 1-s intervals the matrix was searched for severing events. A “severing event” was identified when removed tubulin dimers (state “0”) traced a path to connect the left (protofilament one) and right (protofilament 13) edges of the matrix, separated by one or two vertical rows to account for discontinuities at the seam resulting from the 3 monomer ($1\frac{1}{2}$ dimer) pitch per helical turn. The matrix was shortened after each severing event,

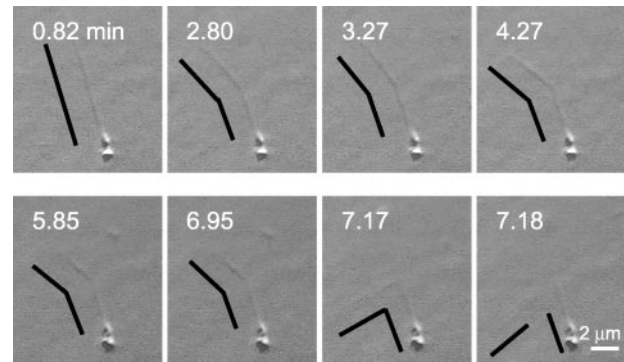


FIGURE 1 VE-DIC images of katanin-mediated severing of an axoneme-nucleated paclitaxel-stabilized microtubule. The initial kink developed at 2.78 min, after which the microtubule bent and straightened for several minutes and was finally severed at 7.18 min. Times are in minutes post-perfusion of 5.7 nM katanin. Black bars to the left of the microtubule highlight the extent of kinking.

removing the severed end and continuing to simulate only the end of the microtubule defined as attached to the axoneme. Because the simulation could “detect” a break in which as few as one row of dimers was removed, only breaks for which the portion of microtubule removed was of “observable” size were reported. An “observable event” was defined as any severing event in which the length of MT removed by severing was at least as long as the shortest experimentally observable severing event, which corresponded to ~ 50 rows of dimers from the MT end.

EXPERIMENTAL RESULTS

In vitro studies of microtubule severing in the presence of katanin and ATP

Within 1 min of perfusion with 290 nM katanin, paclitaxel-stabilized microtubules were seen to kink at apparently random, well-separated locations along their length, while remaining straight elsewhere. The MT segment distal to the axoneme nucleation point rotated about the kink, as if on a hinge. A typical severing event is shown in Fig. 1. The first frame shows the microtubule before kinking, and subsequent frames show representative kinking angles. Note that the MT in frame 3 is less kinked (21°) than in frame 2 (25°) due to fluctuations in the kinking angle. The microtubule kinked at 2.78 min post-katanin perfusion and severed 7.18 min post-katanin perfusion, just before frame 8. The final kinking angle in this particular sequence was $74.3 \pm 2.1^\circ$.

In all cases, each microtubule segment kinked in only one direction and the relative angle between the two MT segments fluctuated stochastically, presumably due to Brownian motion. Microtubules with several kinks often twisted in multiple directions, occasionally bringing a portion of the MT out of the plane of focus. The kinked state, defined as the time from the first discernible kink ($> 5^\circ$), until the microtubule was finally severed, persisted for 1.1 ± 1.7 min ($n = 44$) before the MT was completely severed, and the severed end was then transported away by diffusion into the surrounding fluid.

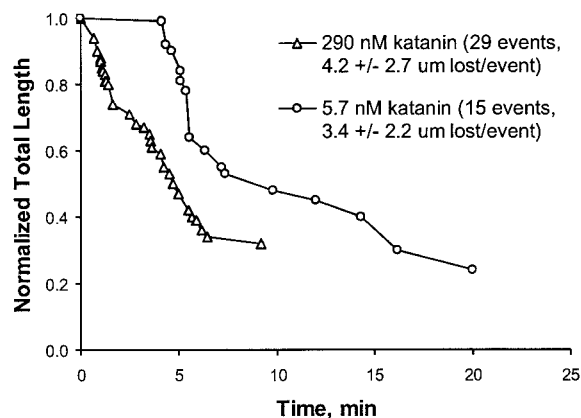


FIGURE 2 Microtubule survival curve. The total normalized length of remaining microtubule is plotted as a function of time for both in vitro katanin concentrations.

After severing, the remaining microtubule segments were stable with respect to depolymerization, as expected for paclitaxel-stabilized MTs. Of the 22 microtubules severed by 290 nM katanin and the 10 MTs severed by 5.7 nM katanin, the first kinks were observed at 0.62 and 2.60 min post-katanin perfusion, respectively. The time-dependence of microtubule survival at both katanin concentrations (290 nM and 5.7 nM) is shown in Fig. 2. Severing was not complete within the timeframe shown: at the higher concentration 72% of the total MT length had been removed after 10 min, and at the lower concentration 76% of the MT length was removed within 20 min. Several experiments were observed for longer times without observation of further severing events. The 50-fold decrease in katanin concentration resulted in only an approximate doubling of the mean severing times ($t_{290 \text{ nM}} = 3.3 \pm 2.2 \text{ min}$, $t_{5.7 \text{ nM}} = 8.5 \pm 4.9 \text{ min}$). These statistics (and others discussed below) are summarized in Table 1.

The population of microtubules from the six experiments at 290 nM had 22 MTs (total length = 180 μm) that were severed a total of 29 times. The population of microtubules from the nine 5.7 nM katanin experiments yielded 10 MTs (total length = 73 μm) and a total of 15 severing events. The mean distance between severing sites was $4.2 \pm 2.7 \mu\text{m}$ ($n = 29$) with 290 nM katanin and $3.7 \pm 2.4 \mu\text{m}$ ($n =$

TABLE 1 Summary of microtubule severing results

	290 nM Katanin	5.7 nM Katanin
Number of assays analyzed	6	9
Number of microtubules	22	10
Number of severing events	29	15
Total microtubule length	180 μm	73 μm
Mean time before severing	$3.3 \pm 2.2 \text{ min}$	$8.5 \pm 4.9 \text{ min}$
Mean time in kinked state	$0.9 \pm 1.5 \text{ min}$	$1.6 \pm 1.9 \text{ min}$
Mean length lost	$4.2 \pm 2.7 \mu\text{m}$	$3.4 \pm 2.2 \mu\text{m}$
Final level of severing	76% complete	72% complete

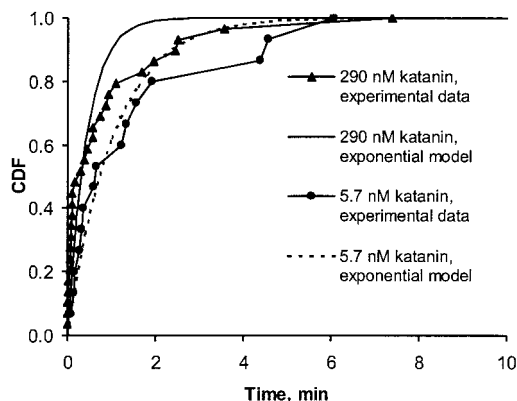


FIGURE 3 Distribution of kinked-state duration. The elapsed time between the formation of each kink and the subsequent break at that location was plotted as a cumulative distribution for both in vitro data sets. An exponential proves a satisfactory fit to both curves [$k_{\text{kb}, 290 \text{ nM}} = 0.039 \text{ s}^{-1}$, $p_{\text{exp}, 290 \text{ nM}} = 0.52$; $k_{\text{kb}, 5.7 \text{ nM}} = 0.016 \text{ s}^{-1}$, $p_{\text{exp}, 5.7 \text{ nM}} = 0.82$].

15) with 5.7 nM katanin, and the shortest segment removed from the end of a microtubule was $0.40 \mu\text{m}$ (~ 50 rows of tubulin) in length. The mean separations were not different by t -test ($\alpha = 0.05$), so the mean length of MT lost was unchanged despite a 50-fold change in katanin concentration. The cumulative effect of removal of lengths shorter than $0.40 \mu\text{m}$ was not detectable.

Several initial experiments with native sea urchin katanin at two concentrations intermediate to those discussed above showed a total of 36 severing events separated by a mean distance of 2.2 and $4.7 \mu\text{m}$ (data not shown). Severing was 65% and 82% complete, and the MT survival curves were of the same shape as the curves from the recombinant sea urchin katanin shown in Fig. 2. Severing by recombinant katanin was chosen for comparison to models because of the larger concentration range and the greater number of experiments.

Analysis of time between kink and break

To examine the kinetics of the transition from the kinked to the broken state, the length of time that each microtubule spent kinked before breaking was plotted as a cumulative distribution function (CDF) for both concentrations. First-order transitions (single-step reactions) follow an exponential distribution when plotted as a CDF, whereas more complex functional forms, for example the gamma distribution, better characterize multiple-step reactions. Curve-fitting an exponential function to the kinking time data gave a satisfactory fit [$p_{\text{exp}, 290 \text{ nM}} = 0.52$, $p_{\text{exp}, 5.7 \text{ nM}} = 0.82$] (Fig. 3), so the hypothesis that the transition from kinked to broken states is a single-step process cannot be rejected. The apparent first-order rate constant for the higher katanin concentration was approximately double that of the lower concentration, [$k_{\text{kb}, 290 \text{ nM}} = 3.9 \times 10^{-2} \text{ s}^{-1}$, $k_{\text{kb}, 5.7 \text{ nM}} =$

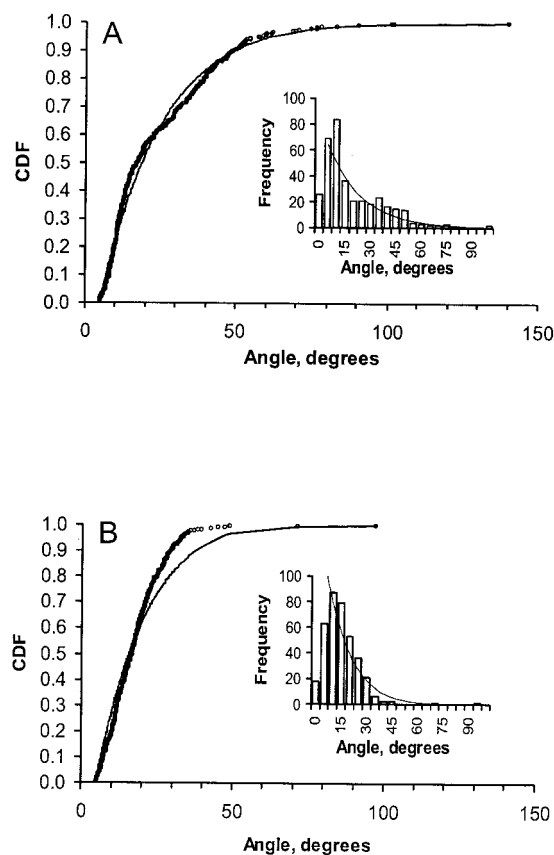


FIGURE 4 Observed kinking angles and diffusion-reaction model fit for microtubules severed by (A) 290 nM katanin [$k_{kb} = 0.039 \text{ s}^{-1}$, $D_r = 16.1 \text{ deg}^2 \text{ s}^{-1}$, $n = 366$, $p_{d-r} = 0.67$] or (B) 5.7 nM katanin [$k_{kb} = 0.016 \text{ s}^{-1}$, $D_r = 4.40 \text{ deg}^2 \text{ s}^{-1}$, $n = 369$, $p_{d-r} = 0.14$]. The diffusion-reaction model was fit to data for angles $>5^\circ$ because of likely underestimation of angles $0-5^\circ$.

$1.6 \times 10^{-2} \text{ s}^{-1}$, different by t -test with $\alpha = 0.05$). However, the mean length of time spent in the kinked state [$t_{290 \text{ nM}} = 0.91 \pm 1.54 \text{ min}$, $t_{5.7 \text{ nM}} = 1.57 \pm 1.89 \text{ min}$] was not different at the two katanin concentrations by t -test ($\alpha = 0.05$). Taken together, the transition from kinked to broken states is apparently first-order and very weakly dependent on katanin concentration, consistent with the breaking of a single noncovalent bond at the hinge point. Thus, in subsequent modeling, the evaluation criteria will include this rate constant as the necessary rate of the final step in the severing reaction.

Analysis of preferred angle distributions

To quantitatively characterize the nature of the kinked state and determine whether any orientations were energetically preferred, an analysis of kinking angles was performed. Kinking angles were measured by sampling one frame every 0.5 s (Fig. 4). Observed angles ranged from 2° (the minimum observable angle) to $>90^\circ$, with an angle of 0°

corresponding to a perfectly straight microtubule. Microtubules kinking out of the plane of focus were not included. While angles of $>90^\circ$ were occasionally observed for one to two frames, analysis of MTs for which these angles persisted for longer times (2 events) suggested that the MT ends had kinked into or out of the plane and these two MTs were not included in this analysis.

If indeed the kinked portion of a microtubule is acting as a hinge about which the distal MT end is freely rotating, then a diffusion-reaction model (see Methods) should predict the frequency with which kinking angles are experimentally observed. In this model, the free end of the kinked MT rotates about a hinge point with rotational diffusivity D_r , and is severed by a first-order reaction with rate constant k_{kb} . Using the values of k_{kb} already determined and minimizing the SSE to find the rotational diffusivity gave $D_{r(290 \text{ nM})} = 16.1 \text{ deg}^2 \text{ s}^{-1}$ and $D_{r(5.7 \text{ nM})} = 4.40 \text{ deg}^2 \text{ s}^{-1}$ [different by t -test, $\alpha = 0.05$], so D_r is only weakly dependent on katanin concentration.

The probabilities of fit for the diffusion-reaction model were 0.67 and 0.14 for the higher and lower katanin concentrations, respectively. Given these probabilities, a model in which the distal end of kinked microtubules rotates with diffusivity D_r , breaks with rate k_{kb} , and in which all kinking angles have equal energy cannot be rejected as a valid description of kinking behavior. Additionally, there are no angles that are significantly under- (or over-) predicted at both concentrations, which would be expected if specific angles were energetically favorable (or unfavorable).

SIMULATION RESULTS

Simulations of defect-free models

To test theoretical models of microtubule severing, several characteristics of the MT survival curve (Fig. 2) and the severing process were chosen for comparison. The results from each simulation of severing were plotted as an MT survival curve, compared to the experimental curve, and evaluated based on the following criteria. An appropriate model will satisfy all five criteria at both katanin concentrations, using a single parameter set to simulate the experimentally observed number and average length of microtubules:

1. The *overall shape* of the curve;
2. The *incompleteness* of the severing reaction;
3. The *total number* of severing events relative to the microtubule population;
4. The *mean length removed* in each severing event;
5. The *rate constant of the final step* in the severing reaction.

In simulations, the final step of the severing reaction is the removal of the last tubulin dimer before breaking. This rate

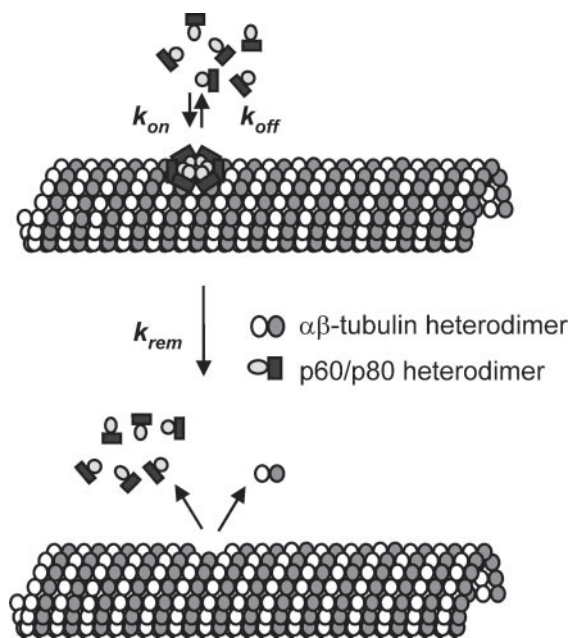


FIGURE 5 Microtubule-severing simulation model and associated parameters. The pseudo-first-order rate constant for the process of katanin hexamer formation and binding to the microtubule, k_{on} , the first-order rate constant for katanin dissociation without tubulin removal, k_{off} , and the first-order rate constant for tubulin dimer removal by katanin, k_{rem} , are illustrated above.

should correspond to the experimentally observed rate of the transition from the kinked state to the broken state, k_{kb} .

The basic model and its associated parameters are illustrated in Fig. 5, in which katanin is shown as six p60/p80 heterodimers binding as a hexamer to the outside of a defect-free microtubule. The second-order rate constant for katanin binding to tubulin, k_{on} [$M^{-1} s^{-1}$], was multiplied by the katanin concentration to yield a pseudo-first-order rate constant. This rate constant was used to calculate p_{on} , the probability of katanin binding to the dimer in the current simulated time increment. Once bound, katanin was allowed to either dissociate alone or dissociate along with a single tubulin dimer, thus removing one tubulin dimer from the lattice. The rate of katanin dissociation from the lattice without tubulin removal, k_{off} [s^{-1}], was used to calculate the probability, p_{off} , and the rate of katanin-mediated tubulin removal, k_{rem} [s^{-1}], was used to calculate the probability, p_{rem} . For simplicity, katanin hexamer formation on the lattice was modeled as a single-step process, although the mechanism of formation is unknown. Results from simulations in which katanin hexamer formation was modeled as a six-step process with equal rate constants were indistinguishable from single-step binding models with the exception of the size of k_{on} . At the other extreme, highly cooperative binding could be approximated using the rate constant for the rate-limiting step.

These defect-free models implicitly assume that katanin binds to the outside of the lattice, because all tubulin dimers

are assumed to be equally accessible to free katanin and diffusion inside the microtubule lumen is predicted to be slow (Odde, 1998). Due to the size of the katanin hexamer relative to tubulin, katanin hexamers were not allowed to bind to adjacent tubulin dimers. At each time step the lattice was checked for breaks, and shortened appropriately.

Defect-free model

The simplest model was one in which tubulin dimers were assumed to reside in a defect-free lattice. Model parameters included k_{on} , k_{off} , and k_{rem} , and were the same for all dimers. Katanin was assumed to remove a single tubulin dimer with each cycle of activity, and the katanin concentration was held constant throughout the simulations. Parameter values were varied independently to minimize the SSE between simulated and experimental MT survival curves; >35 different parameter sets were investigated. The optimized simulation parameters for 290 nM katanin severing [$k_{on} = 2 \times 10^4 M^{-1} s^{-1}$, $k_{rem} = 1 \times 10^{-2} s^{-1}$, $k_{off} = 1 \times 10^{-2} s^{-1}$] were used to obtain the 10 simulated MT survival curves shown in Fig. 6 A.

This model fails four of the five evaluation criteria. The first severing events occurred ~ 3 min post-katanin perfusion followed by a precipitous drop in MT length and complete severing within 10 min. In contrast, the *in vitro* results were characterized by a severing event within 41 s post-perfusion, a gradual decrease in total MT length, and incomplete severing (24% of total length remained). The predicted mean number of observable breaking events is 66 ± 6 events ($n = 10$), compared to the 29 events observed experimentally. The mean MT length lost per simulation is $2.7 \pm 0.3 \mu m$, and the experimentally observed mean falls outside the 95% confidence limits set by the simulations. Random fluctuations due to the stochastic nature of this process do not account for these discrepancies. The rate constant for removal of the final tubulin dimer [$k_{rem} = 1 \times 10^{-2} s^{-1}$] was within a factor of four of the rate constant for the transition from the kinked state to the broken state [$k_{kb} = 3.9 \times 10^{-2} s^{-1}$]. An example of a defect-free lattice during simulation with these optimized parameters is shown in Fig. 7. Note the missing dimers all along the length of the MT, not just at the severing locations.

The simulation parameters were also varied independently to find optimal values for the 5.7 nM katanin data set, using the appropriate initial MT lengths [$k_{on} = 2 \times 10^5 M^{-1} s^{-1}$, $k_{rem} = 5 \times 10^{-2} s^{-1}$, $k_{off} = 5 \times 10^{-2} s^{-1}$] (Fig. 6 B). Although the resulting overall affinity for katanin to tubulin dimers is not dramatically different (katanin-tubulin binding affinity differed by less than an order of magnitude), using the optimized parameter set for one concentration to simulate severing at the other concentration did not give acceptable results (data not shown).

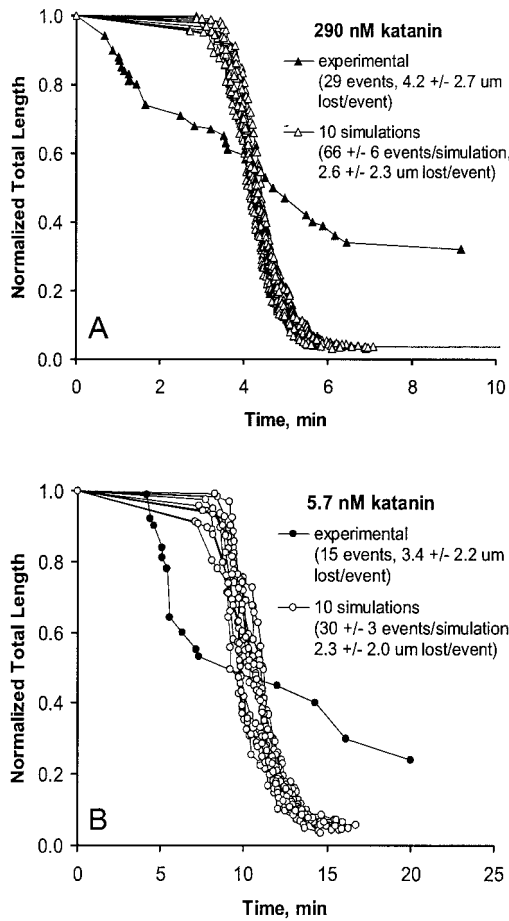


FIGURE 6 Defect-free simulation results. Simulated MT length is plotted as a function of time for (A) 10 simulations with rate constants optimized to best fit the 290 nM katanin experimental data [$k_{on} = 2 \times 10^4 M^{-1} s^{-1}$, $k_{rem} = 1 \times 10^{-2} s^{-1}$, $k_{disoc} = 1 \times 10^{-2} s^{-1}$] and (B) 10 simulations with rate constants optimized to best fit the 5.7 nM katanin data [$k_{on} = 2 \times 10^5 M^{-1} s^{-1}$, $k_{rem} = 5 \times 10^{-2} s^{-1}$, $k_{off} = 5 \times 10^{-2} s^{-1}$]. Note that the final level of simulated severing appears to be <100% because only events that removed MT segments large enough for experimental observation were plotted.

Katanin-inactivation model

Because the defect-free model was unable to account for incomplete severing, and because it is possible for proteins to become adsorbed to the perfusion cell walls during the course of an assay, the simulated concentration of free katanin was allowed to decrease to simulate its inactivation by either a zero- or first-order reaction with rate constant k_{inact} . The results of katanin inactivation by first-order reaction are shown in Fig. 8. Values for k_{on} , k_{off} , and k_{rem} remained unchanged in the simulation shown, although the parameter space was once again fully explored. Inactivation allowed the prediction of incomplete severing and improved the overall shape of the curve. However, the first severing events were further delayed (to almost 4 min post-perfusion in the simulations shown) and inactivation rates appropriate

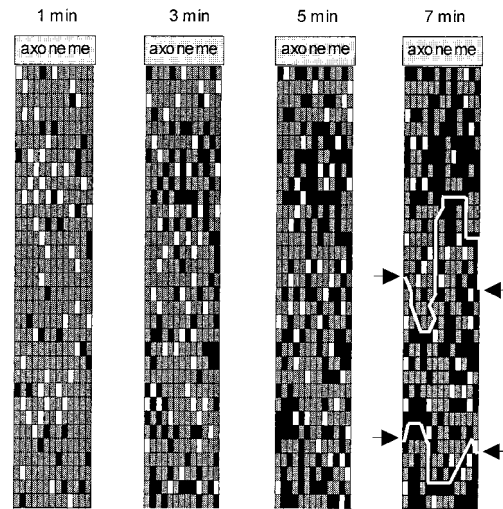


FIGURE 7 A defect-free microtubule lattice during simulation. The first 30 rows of a defect-free microtubule are shown at several times during the simulation. Gray boxes represent intact tubulin, white boxes represent tubulin with katanin hexamer bound, and black boxes represent locations where tubulin dimers have been removed. A break is present if a missing dimer in the first protofilament is connected to a missing dimer one or two rows beneath it (to account for the three-turn helix) in the 13th protofilament. Here, the first severing events in this region of the microtubule are shown in the fourth lattice, as denoted by arrows.

for 290 nM katanin ($k_{inact} \sim 10^{-3} s^{-1}$) resulted in complete elimination of severing at the 5.7 nM concentration. Katanin inactivation by a zero-order reaction gave similar results (data not shown). It was concluded that inactivation alone

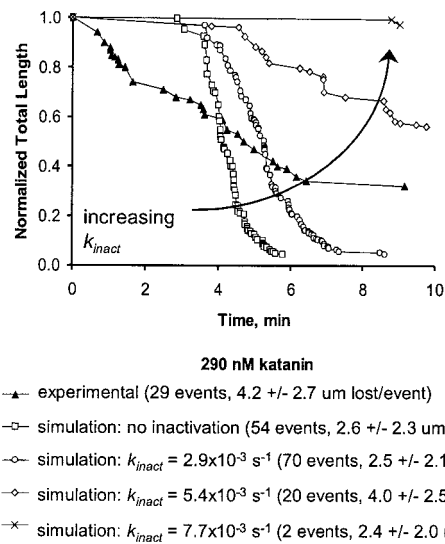


FIGURE 8 Katanin-inactivation simulation results. Simulated MT length as a function of time is shown for increasing first-order katanin inactivation rates, using the optimized defect-free rate constants. For clarity, results from only one simulation are shown; simulation-to-simulation variability is similar to that in Fig. 6 A.

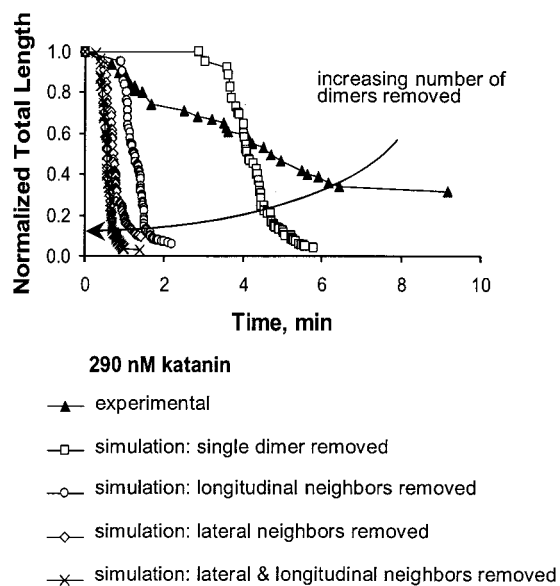


FIGURE 9 Multiple-dimer removal simulation results. Tubulin dimers were removed singly and in variously sized groups; the results of representative simulations are shown. [□, single dimer removed (54 events); ○, removal of the center dimer and longitudinal neighbors (3 dimers/cycle, 63 events); ◇, removal of the center dimer and lateral neighbors (3 dimers/cycle, 73 events); ×, removal of the center dimer and its lateral and longitudinal neighbors (5 dimers/cycle, 66 events)]. For clarity, results from only one simulation are shown; simulation-to-simulation variability is similar to that in Fig. 6 A.

could not account for the experimentally observed characteristics of in vitro katanin-mediated severing.

Multiple-dimer removal model

Because katanin forms hexameric rings in the presence of microtubules (Hartman and Vale, 1999) and has been hypothesized to act as a larger complex of multiple hexamers (McNally, 2000), it may be physiologically possible to remove multiple dimers with each cycle of activity. Removal of multiple dimers would reduce the number of steps necessary for severing and should allow prediction of early severing events. Various sized groups of tubulin dimers were removed using the same optimized rate constants as before; three examples are shown in Fig. 9. Simulations showed that removing groups of tubulin dimers shifted the microtubule survival curve to earlier times, but does not change the shape, the overall level of severing, or the number of predicted events even when all the parameters are independently adjusted to provide the best possible fit to the experimental data. The combination of multiple dimer removal plus katanin inactivation showed no improvement over either model alone.

Cooperative-removal model

The microtubule lattice is stabilized by interactions of tubulin with its lateral and longitudinal neighbors. It has been

suggested by Dye and co-workers that the rate-limiting step for tubulin dissociation is removal of the first dimer; subsequent dimers dissociate more rapidly because of the loss of stabilizing tubulin-tubulin contacts (Dye et al., 1992). Thus, once a dimer has been removed it may become easier for katanin to remove its neighbors. This modification was made by increasing the katanin-mediated tubulin-removal rate (k_{rem}) for the neighbors of missing dimers. Assuming that longitudinal bonds between dimers are twice as strong as those between lateral neighbors (Mandelkow et al., 1991), k_{rem} for a particular dimer was increased by the same factor upon removal of each subsequent neighbor (four lateral bonds and two longitudinal bonds per dimer). Any dimer missing all four of its neighbors was removed without regard to its katanin binding state. The factor by which k_{rem} increased upon removal of each subsequent neighbor was varied from 10 to 2×10^4 (corresponding to a change in tubulin-tubulin binding energy of $\sim 2.3\text{--}10 k_B T$) without satisfying the model criteria.

While severing is shifted to earlier times (compared to the simplest defect-free model) it does not show improved characteristics over simpler models (data not shown). The addition of an optimized inactivation term did improve the shape and overall severing level in the same manner as for earlier models, but did not result in improvement above the performance of previous models with respect to severing at both katanin concentrations (data not shown).

Simulations of defect-containing models

Defect-containing model

Because defect-free lattice models were unable to predict the experimentally observed severing dynamics, a defect-containing lattice model was proposed. Physiologically, lattice defects could be the result of changes in protofilament number (Chrétien et al., 1992), failure to incorporate tubulin during assembly, or tubulin loss after assembly, any of which could cause the weakening of tubulin-tubulin bonds in the region of the defect, making it easier for katanin to remove surrounding dimers. The model consisted of an MT lattice that began with “defects” placed randomly throughout the lattice. These defects were not holes in the lattice, but rather were subunits with a higher removal rate than other dimers. The parameters for this model included k_{on} , k_{rem} , and k_{off} , as before, but also added three new parameters: $k_{\text{rem def}}$ [s^{-1}], the rate of katanin-mediated tubulin removal within a defect, *defect level* [$\frac{\text{defects}}{\text{dimer}}$], the frequency of lattice defects, and *defect size*, the number of dimers in each direction from the center that are affected by the new parameter, $k_{\text{rem def}}$.

Simulation results using the new optimized parameter set are shown in Fig. 10. This parameter set [$k_{\text{on}} = 2 \times 10^6 \text{ M}^{-1} \text{ s}^{-1}$, $k_{\text{off}} = 0 \text{ s}^{-1}$, $k_{\text{rem}} = 5 \times 10^{-3} \text{ s}^{-1}$, $k_{\text{rem def}} = 1 \times 10^{-1} \text{ s}^{-1}$, *defect level* = $1 \times 10^{-3} \frac{\text{defects}}{\text{dimer}}$, *defect size* =

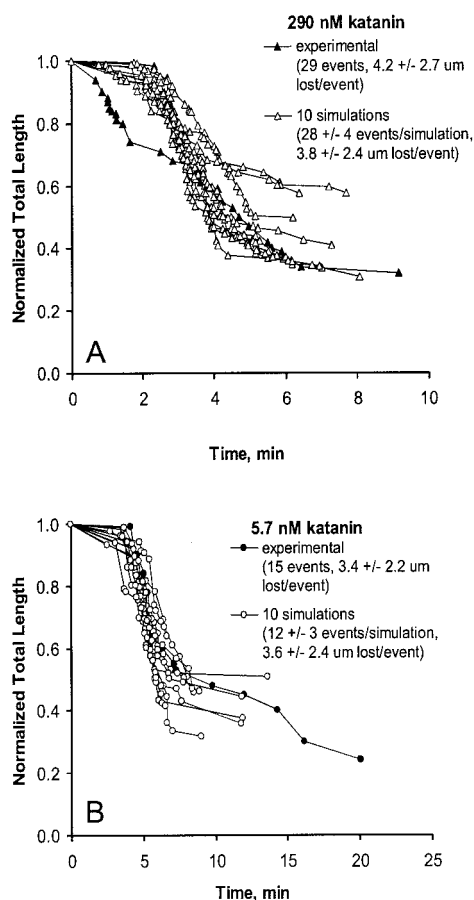


FIGURE 10 Simulation results for the defect-containing model. Simulations at both katanin concentrations used the same set of optimized rate constants: [$k_{\text{on}} = 2 \times 10^6 \text{ M}^{-1} \text{ s}^{-1}$, $k_{\text{off}} = 0 \text{ s}^{-1}$, $k_{\text{rem}} = 5 \times 10^{-3} \text{ s}^{-1}$, $k_{\text{rem def}} = 1 \times 10^{-1} \text{ s}^{-1}$, $\text{defect level} = 1 \times 10^{-3} \text{ defects/dimer}$, $\text{defect size} = 2$]. Ten representative simulated MT survival curves are shown in (A) 290 nM katanin [$p_{\text{defects 290 nM}} = 0.16$, $n = 100$ simulations], and (B) 5.7 nM katanin [$p_{\text{defects 5.7 nM}} = 0.81$, $n = 100$ simulations].

2] allowed severing at both katanin concentrations and was able to predict both the appropriate number of breaks and incomplete severing within the observation time. A defect level of 0.001 corresponds to one defect per 0.6 μm of MT length. The value chosen for k_{off} did not have a significant effect on the results and was set to zero, reducing the number of model parameters.

Simulations with this parameter set predicted 27 ± 4 observable breaks ($n = 100$), $57 \pm 7\%$ completion of

severing, and a mean severed length of $3.7 \pm 2.4 \mu\text{m}$ [versus 29 breaks, 76% complete, and $4.2 \pm 2.7 \mu\text{m}$ in vitro] (Fig. 10 A). At the lower concentration, simulations predicted 12 ± 3 observable breaks ($n = 100$), $57 \pm 11\%$ completion of severing, and a mean severed length of $3.4 \pm 2.5 \mu\text{m}$ [versus 15 breaks, 74% complete, and $3.4 \pm 2.2 \mu\text{m}$ in vitro] (Fig. 10 B). The rate constants for the removal of individual tubulin dimers were $k_{\text{rem}} = 0.005 \text{ s}^{-1}$ outside defects and $k_{\text{rem def}} = 0.1 \text{ s}^{-1}$ within defects. These two rates bracket the experimentally observed rates for the transition from kinked to broken microtubules [$k_{\text{kb, 290 nM}} = 0.039 \text{ s}^{-1}$ and $k_{\text{kb, 5.7 nM}} = 0.016 \text{ s}^{-1}$]. The model results for defect-free and defect-containing models are compared in Table 2. The simulation-to-simulation variability in defect-containing simulations is larger than that seen for simulations of defect-free lattices, and comparison to the data shows that the model cannot be rejected as a valid representation of katanin behavior [$p_{\text{defects, 290 nM}} = 0.16$, $p_{\text{defects, 5.7 nM}} = 0.81$]. The addition of katanin inactivation and cooperative-removal of dimers did not significantly improve the simulation's performance (data not shown).

DISCUSSION

Kinking and severing of mechanically unconstrained microtubules in vitro occurred at spatially well-separated, katanin concentration-independent locations along the length of microtubules, so that proximal segments of microtubule often remained attached to the axoneme even when exposed to katanin for relatively long periods of time. Computer simulations showed that models assuming a uniform, defect-free MT lattice were unable to simultaneously predict each of these characteristics. In contrast, simulations of a model assuming a defect-containing lattice were shown to correctly predict the experimentally observed breaking rates, spatial frequency and number of severing events, and the final level of severing, while using a single set of parameter values at both katanin concentrations. Consistent with these results is the hypothesis that katanin exploits local defects and promotes loss of tubulin at the defect site until the two microtubule segments are held together so weakly that mechanically unconstrained MTs kink at the defect site. A single, random event, whose rate is insensitive to katanin concentration, allows the distal and proximal segments to then dissociate.

TABLE 2 Comparison of experimental and simulated results

	290 nM Katanin		5.7 nM Katanin	
	Experiment	Simulation	Experiment	Simulation
Incompleteness of reaction	28%	$43 \pm 7\%$	24%	$43 \pm 11\%$
Total number of events	29	27 ± 4	15	12 ± 3
Mean length removed	$4.2 \pm 2.7 \mu\text{m}$	$3.8 \pm 2.4 \mu\text{m}$	$3.7 \pm 2.4 \mu\text{m}$	$3.6 \pm 2.4 \mu\text{m}$
Rate constant of final step	0.039 s^{-1}	$0.1 - 0.005 \text{ s}^{-1}$	0.016 s^{-1}	$0.1 - 0.005 \text{ s}^{-1}$

Katanin activity and lattice defects

The argument against a defect-free microtubule lattice is strengthened by qualitative observations of the microtubule during lattice simulations. Simulations of defect-free models showed katanin removing tubulin dimers from all along the length of the MT, and resulted in a MT so structurally compromised that it would tend to disintegrate (Fig. 7). In contrast, MTs *in vitro* were observed to undergo localized kinking and breaking, separated by structurally intact MT segments. A defect-containing lattice model concentrates katanin activity at defect locations and offers an explanation for the incompleteness of severing: if katanin acts at infrequent defect locations, then severing activity will cease (or slow) once katanin has operated on all the defects. The requirement for defects also lends some credibility to the hypothesis that katanin acts from within the microtubule (McNally, 2000). Defects present in the form of “holes” in the lattice could allow katanin dimers to enter the microtubule at points along its length. Because diffusion within the tube is slow for molecules that can bind to the MT lumen (Odde, 1998), katanin would remain localized to its entrance points, resulting in severing near the defects.

One possible defect-containing model was chosen for simulation, but there were several others that are potentially viable. For example, one could assume that katanin acts as a cooperative group of hexamers, which could maintain multiple contacts to the MT, even as tubulin dimers were removed (McNally, 2000). This would eliminate the need for katanin to dissociate and reattach after each cycle of activity, and would concentrate the activity to a single site on the MT. We do not favor this assumption, because in such a katanin-mediated localization mechanism the separation between severing sites would be concentration-dependent in a manner not observed experimentally. Instead, the defect-containing model that was chosen for simulation assumed that katanin dissociated from the MT with each cycle of activity. Localization of activity was achieved by increasing the off-rate for katanin-mediated tubulin removal at the sites of randomly placed defects. Biophysically, these defects could represent places in the lattice where the free energy of tubulin dimers is increased due to disruptions in tubulin-tubulin contacts, for example by changes in protofilament number.

Experimental defect frequency

Katanin activity could be concentrated around defects caused by changes in protofilament number that frequently occur within a single microtubule (Chrétien et al., 1992; Arnal and Wade, 1995; Díaz et al., 1998). Changes in protofilament number would disrupt tubulin-tubulin bonds near the site of the defect, making it easier for katanin to remove tubulin dimers. The reported frequency of these defects in GDP-tubulin microtubules without stabilizing

drugs covers the range from one defect per 3 μm of MT length to one defect per 35 μm of MT length (Chrétien et al., 1992; Arnal and Wade, 1995). In contrast, the predicted defect frequency for the defect-containing model presented here was one defect for every 0.6 μm of microtubule length, more frequent by a factor of between 5 and 50. However, these same studies showed that the addition of paclitaxel to MTs after assembly doubled the defect frequency (Arnal and Wade, 1995). Additionally, the frequency of defects is sensitive to Mg^{2+} concentration, the length of time between paclitaxel addition and observation, the initial protofilament number of the microtubules, and the initial tubulin dimer concentration (Chrétien et al., 1992; Arnal and Wade, 1995; Chrétien and Fuller, 2000), all of which make direct comparison of model predictions to experimental results difficult. Finally, the half-periodicity of moiré patterns used to determine the number of protofilaments varies by as much as 10% (Hyman et al., 1995; Chrétien et al., 1998), suggesting that closely spaced defects would not likely be differentiated by this technique, thus skewing the mean distance between protofilament number changes toward longer distances. Taken together, the experimental values for changes in protofilament number give an upper bound for the distance between lattice defects due to changes in protofilament number, but not a definitive value.

A lower bound for the distance between microtubule lattice defects can be estimated from the run lengths of a recently developed kinesin mutant. This kinesin has a mean run length of 6.6 μm , more than four times longer than wild-type (Thorn et al., 2000). The increase in run-length for these mutants can be assumed to reduce the probability of random detachment, thereby increasing the proportion of detachments due to encountering defects or other obstacles. Because of its plus-end directed motor activity along a single protofilament, kinesin would detach only in response to decreases in protofilament number, not increases. Assuming that protofilament number decreases are found in equal proportion to increases, the minimum distance between defects can be calculated to be one defect every 0.25 μm of MT length (6.6 $\mu\text{m}/13$ protofilaments/2). The defect frequency predicted by simulations of defect-containing MT lattices (one every 0.6 μm) is within the range defined by experimental observations of changes in protofilament number (less than one every 3 μm) and kinesin processivity (more than one every 0.25 μm). However, to more rigorously evaluate the predicted defect frequency, a better understanding of the actual defect frequency and type in microtubules, both with and without microtubule stabilizing drugs, is necessary.

Analysis of kinking, an intermediate state in the severing reaction

In the current assay microtubules were observed to enter a kinked state, followed by breaking at the kink. The cause of

kinking is unknown. One possibility is that removal of tubulin from the MT lattice allows the remaining protofilament(s) to curve outward, as has been observed at the tips of disassembling microtubules (Simon and Salmon, 1990; Mandelkow et al., 1991; Müller-Reichert et al., 1998). It is also possible that katanin itself, through its ATPase activity, directly exerts forces on the MT to cause it to kink. A third possibility is that kinking is a result of thermal forces acting on an MT lattice weakened by tubulin removal, causing the MT to bend at its weakest point. The case for this final possibility is strengthened because no preferred kinking angles were detected: simulations of distal segments of kinked microtubules undergoing rotational diffusion about a hinge point without any preferred angles of orientation were indistinguishable from simulations of the diffusion around a hinge point *with* preferred angles, as long as the difference in energy between angles was assumed to be $<3 k_B T$ (simulations not shown).

The microtubule segments on either side of the kink appear to be held together by one or more intact protofilaments acting as a hinge. The hinge region could be short, with a single protofilament connecting the two MT segments, and achieved by removal of as few as 12 dimers. The existence of a short, single protofilament hinge region is supported by the first-order kinetics of the transition from the kinked state to the broken state, which suggest that the kinked MT can be severed by one final cycle of katanin activity or by outside forces acting in a single step. The very weak dependence of time spent in the kinked state on katanin concentration suggests that the final step is mediated by outside forces. The second possibility is that there is a multiple-protofilament hinge, which would tend to be less flexible than a single-protofilament hinge because of its remaining lateral tubulin-tubulin bonds, and would therefore need to be longer than a single-protofilament hinge to achieve the large kinking angles observed in some microtubules. A longer hinge region would also require the removal of a significantly larger number of tubulin dimers than the defect-containing model.

Implications for severing in vivo

One implication of defect-localization of katanin activity would be the in vivo targeting of “old,” or deficient, MTs for disassembly: high defect rates could lead to high severing rates and an increase in the rate of MT turnover. Using katanin, cells could sense “high energy” states in the polymer (created by lattice defects) and then katanin could assist in the breakdown at these “high energy” points. The targeting of katanin activity to defects would also allow the cell to maintain a specific average MT length within the cell by modulating the frequency of defects. Ahmad and co-workers reported evidence that katanin regulates MT length even after MTs are released from the centrosome (Ahmad et al., 1999). One possible mechanism for MT length regulation is

by increasing the defect frequency to decrease the average MT length, and decreasing the frequency to increase average MT length throughout the cell.

Finally, it would be interesting to determine whether katanin has intrinsic curvature sensitivity, allowing it to target curved microtubules in vivo, and to act as a mechanical/chemical signal transducer. The link between curved MTs and MT breaking in living cells suggests that MT curvature may modulate severing in vivo (Waterman-Storer and Salmon, 1997; Odde et al., 1999). How could this be accomplished? Increased curvature, caused by microtubule motors, actomyosin cortical flow, or mechanical deformation of the cell could increase the number of microtubule defects, in turn increasing the number of katanin severing locations. Alternatively, increased microtubule curvature could increase katanin activity at pre-existing defects by creating a katanin binding site with a higher katanin affinity. Further work needs to be done to determine to what extent mechanical stress within the microtubule lattice modulates katanin activity.

The authors thank Jim Hartman and Ron Vale for their generous gift of katanin, Frank McNally for providing katanin used in preliminary experiments, and Danny Weitz and Eric Schroeder-Freshette for technical assistance in the experimental work.

This work was supported by NSF Grant BES 9984955 and by a grant from NASA through the Michigan Space Grant Consortium.

REFERENCES

- Ahmad, F. J., W. Yu, F. J. McNally, and P. W. Baas. 1999. An essential role for katanin in severing microtubules in the neuron. *J. Cell Biol.* 145:305–315.
- Arnal, I., and R. H. Wade. 1995. How does taxol stabilize microtubules? *Curr. Biol.* 5:900–908.
- Bell, C. W., C. Fraser, W. S. Sale, W.-J. Tang, and I. R. Gibbons. 1982. Preparation and purification of dynein. *Methods Cell Biol.* 24:373–397.
- Chrétien, D., H. Flyvbjerg, and S. D. Fuller. 1998. Limited flexibility of the inter-protofilament bonds in microtubules assembled from pure tubulin. *Eur. Biophys. J.* 27:490–500.
- Chrétien, D., and S. D. Fuller. 2000. Microtubules switch occasionally into unfavorable configurations during elongation. *J. Mol. Biol.* 298:663–676.
- Chrétien, D., F. Metoz, F. Verde, E. Karsenti, and R. H. Wade. 1992. Lattice defects in microtubules: protofilament numbers vary within individual microtubules. *J. Cell Biol.* 117:1031–1040.
- Crank, J. 1975. *The Mathematics of Diffusion*. Oxford University Press, Oxford.
- Díaz, J. F., J. M. Valpuesta, P. Chacón, G. Diakun, and J. M. Andreu. 1998. Changes in microtubule protofilament number induced by taxol binding to an easily accessible site. *J. Biol. Chem.* 273:33803–33810.
- Dye, R. B., P. F. Flicker, D. Y. Lien, and R. C. Williams, Jr. 1992. End-stabilized microtubules observed in vitro: stability, subunit interchange, and breakage. *Cell Motil. Cytoskel.* 21:171–196.
- Hartman, J. J., J. Mahr, K. P. McNally, K. Okawa, A. Iwamatsu, S. Thomas, S. Cheesman, J. Heuser, R. D. Vale, and F. J. McNally. 1998. Katanin, a microtubule-severing protein, is a novel AAA ATPase that targets to the centrosome using a WD40-containing subunit. *Cell.* 93:277–287.

- Hartman, J. J., and R. D. Vale. 1999. Microtubule disassembly by ATP-dependent oligomerization of the AAA enzyme katanin. *Science*. 286:782–785.
- Hyman, A. A., D. Chrétien, I. Arnal, and R. H. Wade. 1995. Structural changes accompanying GTP hydrolysis in microtubules: information from a slowly hydrolyzable analogue guanylyl-(α , β)-methylenediphosphate. *J. Cell Biol.* 128:117–125.
- Janosi, I. M., D. Cretien, and H. Flyvbjerg. 1998. Modeling elastic properties of microtubule tips and walls. *Eur. Biophys. J.* 27:501–513.
- Lohret, T. A., F. J. McNally, and L. M. Quarmby. 1998. A role for katanin-mediated axonemal severing during *Chlamydomonas* deflagellation. *Mol. Biol. Cell.* 9:1195–1207.
- Mandelkow, E.-M., E. Mandelkow, and R. A. Milligan. 1991. Microtubule dynamics and microtubule caps: a time-resolved cryo-electron microscopy study. *J. Cell Biol.* 114:977–991.
- McNally, F. J. 2000. Capturing a ring of samurai. *Nat. Cell Biol.* 2:E4–E7.
- McNally, F. J., K. Okawa, A. Iwamatsu, and R. D. Vale. 1996. Katanin, the microtubule-severing ATPase, is concentrated at centrosomes. *J. Cell Sci.* 109:561–567.
- McNally, F. J., and R. D. Vale. 1993. Identification of katanin, an ATPase that severs and disassembles stable microtubules. *Cell.* 75:419–429.
- Müller-Reichert, T., D. Chrétien, F. Severin, and A. A. Hyman. 1998. Structural changes at microtubule ends accompanying GTP hydrolysis: information from a slowly hydrolyzable analogue of GTP, guanylyl (α , β)-methylenediphosphate. *PNAS.* 95:3661–3666.
- Odde, D. J. 1998. Diffusion inside microtubules. *Eur. Biophys. J.* 27:514–520.
- Odde, D. J., L. Ma, A. H. Briggs, A. DeMarco, and M. W. Kirschner. 1999. Microtubule bending and breaking in living fibroblast cells. *J. Cell Sci.* 112:3283–3288.
- Simon, J. R., and E. D. Salmon. 1990. The structure of microtubule ends during the elongation and shortening phases of dynamic instability examined by negative-stain electron microscopy. *J. Cell Sci.* 96:571–582.
- Thorn, K. S., J. A. Ubersax, and R. D. Vale. 2000. Engineering the processive run length of the kinesin motor. *J. Cell Biol.* 151:1093–1100.
- Vale, R. D. 1991. Severing of stable microtubules by a mitotically activated protein in *Xenopus* egg extracts. *Cell.* 64:827–839.
- Vale, R. D. 2000. AAA proteins: lords of the ring. *J. Cell Biol.* 150:F13–F19.
- Waterman-Storer, C. M., and E. D. Salmon. 1997. Actomyosin-based retrograde flow of microtubules in the lamella of migrating epithelial cells influences microtubule dynamic instability and turnover and is associated with microtubule breakage and treadmilling. *J. Cell Biol.* 139:417–434.